Amplitude attenuation laws of acoustic emission waves in plate structures

Leyes de atenuación de amplitud de las ondas de emisión acústica en estructuras de chapa

Jianchao Zhang[1,2], Shaopu Yang[3], Rujiang Hao[3] and Xiaohui Gu[3]

[1] School of Mechanical, Electronic and Control Engineering, Beijing Jiaotong University, Shangyuancun 3#, Beijing, 100044, China, zhangjianchao@yeah.net
[2] Engineering Training Center, Shijiazhuang Tiedao University, Northeast, Second Inner Ring 17#, Shijiazhuang, 050043, Hebei, China
[3] Institute of Transportation Environment and Safety Engineering, Shijiazhuang Tiedao University, Northeast, Second Inner Ring 17#, Shijiazhuang, 050043, Hebei, China

DOI: http://dx.doi.org/10.6036/8987 | Recibido: 26/09/2018 • Inicio Evaluación: 26/09/2018 • Aceptado: 30/10/2018

RESUMEN

• Aunque la tecnología de emisión acústica se ha utilizado en los ensayos no destructivos de diversas estructuras de placas, su aplicación y desarrollo siguen siendo limitados debido a que las leyes que rigen la atenuación de la amplitud de las ondas de emisión acústica en las estructuras de las placas siguen siendo poco claras. El objetivo de este estudio fue revelar las leyes de atenuación de amplitud de las ondas de emisión acústicas en las estructuras de las placas. Así, en este estudio, el modelo tradicional de atenuación de amplitud, que se presenta en forma de una función exponencial, fue mejorado en referencia a las ondas cilíndricas, y se propuso un modelo de atenuación de amplitud en forma de una función de potencia adecuada para estructuras de placas. Además, se estableció un sistema experimental para la atenuación de las ondas de emisión acústica en placas de aleación de aluminio para verificar experimentalmente el modelo propuesto. Finalmente, se discutieron las leyes de atenuación de amplitud de las ondas de emisión acústicas dentro del campo completo, campo cercano y campo lejano de las estructuras de las placas. Los resultados muestran que las leyes de atenuación de amplitud de las ondas de emisión acústica dentro del campo completo, campo cercano y campo lejano de las estructuras de las placas se ajustan al modelo de función de potencia y se reducen gradualmente a medida que aumenta la distancia de propagación. Además, el modelo de atenuación de amplitud mejorado se corresponde mejor con la tendencia real de atenuación de amplitud dentro del rango de campo cercano de la fuente de emisión acústica que otras formas de modelos de atenuación de amplitud. Específicamente, el modelo tradicional de atenuación de amplitud concuerda con las leyes de atenuación reales de las ondas de emisión acústicas sólo dentro del rango de campo lejano de la fuente de emisión acústica. Los resultados de este estudio proporcionan valiosas referencias para el análisis profundo de las características de propagación de las ondas de emisión acústicas en estructuras de chapa y pueden emplearse en la investigación de nuevos métodos para la localización de fuentes de ondas de emisión acústicas tipo ráfaga basadas en la atenuación de la amplitud acústica.

• **Palabras clave:** Ondas de emisión acústica, Amplitud, Atenuación, Leyes, Chapa.

ABSTRACT

Although acoustic emission technology has been used in the nondestructive testing of various plate structures, its further application and development remain limited because the laws governing the amplitude attenuation of acoustic emission waves in plate structures remain unclear. This study aimed to reveal the amplitude attenuation laws of acoustic emission waves in plate structures. Thus, in this study, the traditional model of amplitude attenuation, which is in the form of an exponential function, was improved in reference to cylindrical waves, and an amplitude attenuation model in the form of a power function suitable for plate structures was proposed. Moreover, an experimental system for the attenuation of acoustic emission waves in aluminum alloy plates was established to experimentally verify the proposed model. Finally, the amplitude attenuation laws of acoustic emission waves within the full field, near field, and far field of plate structures were discussed. Results show that the amplitude attenuation laws of acoustic emission waves within the full field, near field, and far field of plate structures all conform to the power function model and gradually reduce as propagation distance increases. In addition, the improved amplitude attenuation model better corresponds with the actual amplitude attenuation trend within the near-field range of the acoustic emission source than other forms of amplitude attenuation models. Specifically, the traditional model of amplitude attenuation model agrees with the actual attenuation laws of acoustic emission waves only within the far-field range of the acoustic emission source. The results of this study provide valuable references for the profound analysis of the propagation characteristics of acoustic emission waves in plate structures and can be employed in the research of new methods for source localization of burst-type acoustic emission waves based on acoustic amplitude attenuation.

Keywords: Acoustic emission waves, Amplitude, Attenuation, Laws, Plate.

1. INTRODUCTION

Plate structures, including curved surfaces with small curvatures, are common structures in the industrial field and have been widely used to fabricate the main wall panels of products, such as pressure vessels, boilers, and spacecraft. Given that these products are deployed under harsh conditions, including high temperature, high pressure, and corrosion, they are subjected to highly complex local stresses that promote crack generation. Crack generation and expansion rapidly release local source energy to generate stress waves that result in the occurrence of acoustic emission. The elastic wave sources of fluid leakage, friction, and collision in local structures can be considered acoustic emission [1].

Acoustic emission technology has been successfully applied as a nondestructive testing (NDT) method in the safety monitoring of plate structures in the above products [2–5]. A surface displacement signal is generated when stress waves originating from acoustic emission sources are propagated onto the medium surface and detected by the acoustic emission sensor [6]. It is then used to infer the internal status of the material or defect-type changes or to evaluate the severity of defects. Thus, acoustic emission technology exhibits an effect that cannot be replaced by other NDT methods.

The amplitude of acoustic emission waves attenuates as the propagation distance increases. If the attenuation laws of acoustic emission waves propagated in plate structures cannot be controlled, the spacing of acoustic emission sensors and the threshold of the detection system cannot be properly set, and signal errors in damage evaluation and acoustic source positioning cannot be effectively reduced [7–9]. These limitations seriously restrict the application and development of acoustic emission technology in plate structures.

Progress has been achieved in identifying the amplitude attenuation laws of acoustic emission waves [10–13]. Nevertheless, available studies have not been fully considered the different mechanisms, such as diffusion, scattering, and absorption, underlying the attenuation of acoustic emission waves or else have neglected the effects of different structural features (body, plate, and line) of the propagation medium on the form of the energy propagation of acoustic emission waves. The theoretical model of the amplitude attenuation of acoustic emission waves in plate structures continue to deviate from actual attenuation laws. Therefore, a specific detailed analysis and experimental study of the theoretical model of the amplitude attenuation of acoustic emission waves must be conducted in accordance with the concrete structural forms of propagation media.

2. STATE OF THE ART

In recent years, the laws governing the attenuation of acoustic emission waves have been applied in related fields, such as damage monitoring, life prediction, material analysis, and damage positioning [14–17]. Domestic and international scholars have conducted certain in-depth researches from different angles. Näsholm et al. [18] believed that in complex media, such as biological tissues and polymers, acoustic attenuation conforms to the frequency power law. However, these materials are viscoelastic materials. Thus, their acoustic attenuation laws cannot be applied to the elastic materials used in the present study. Capeli et al. [19] used acoustic emission technology to evaluate the instability of snow slope and obtained attenuation coefficients related to frequency by fitting the power spectra of different discrete frequencies at different distances. They studied the attenuation laws of acoustic emission waves from the aspect of frequency but did not analyze the influence of the change in distance on amplitude attenuation. Wang et al. [20] investigated the attenuation conditions of acoustic emission waves at two common structural interfaces and experimentally verified the influence of interfaces on attenuation. This approach, however, is inapplicable in studies on the attenuation of acoustic emission waves in plate structures.

The analysis of amplitude attenuation laws should proceed from factors that influence acoustic emission wave attenuation. These factors mainly include diffusion, scattering, and absorption attenuation. Zhang et al. [21] accurately determined the position of a faulty planetary wheel on the basis of the amplitude attenuation characteristics of acoustic emission waves but deemed that the diffusion attenuation laws of acoustic emission waves presented exponential attenuation with propagation distance. This conclusion warrants further discussion. Manthei et al. [22] provided the relational expression between the amplitude of acoustic emission waves and propagation distance in the context of diffusion attenuation and absorption attenuation. However, their diffusion attenuation laws are applicable only to body structures but not to plate structures.

Wang et al. [23] studied the propagation law of acoustic emission signal of slewing outer ring and thought that the form of signal energy attenuation of outer surface can be described as an exponential attenuation. Smith et al. [24] proposed using the attenuation of acoustic emission waves to monitor the deformation of buried pipes and posited that the amplitude attenuation of acoustic emission waves is in the form of an exponential function. Li et al. [25] believed that energy, vibration amplitude, duration, and ringing count of the acoustic emission wave amplitude of steel strands embedded in concrete all present exponential function attenuation with increasing propagation distance. The slewing outer ring, buried pipe and steel strand investigated by Wang et al. [23], Smith et al. [24] and Li et al. [25] can be approximated as linear structures and can be said as not experiencing diffusion attenuation. The mechanism underlying propagation under this condition is different from that underlying propagation of acoustic emission waves in plate structures. Therefore, the suitability of the traditional exponential attenuation model for plate structures requires further study.

Some studies focused on the attenuation laws of acoustic emission waves in plate structures. Tang et al. [26] tested the Lamb wave propagation property of carbon-fiber-reinforced composite laminated plate. However, they only qualitatively analyzed the attenuation characteristics of the amplitude and energy of waves with different frequencies and did not propose an attenuation law formula. Sabzevari et al. [27] only considered diffusion attenuation factor and neglected the effects of factors, such as scattering attenuation and absorption attenuation, when studying the acoustic emission source positioning of a composite board at an airplane nose and thus failed to fully reflect the attenuation laws of acoustic emission waves in plate structures. Hafizi et al. [28] applied the acoustic emission attenuation method to monitor damages in fiberglass reinforced composite laminates. However, they directly adopted the exponential functional formula of the amplitude attenuation and did not conduct related derivations and verifications. Asamene et al. [29] studied the attenuation laws of acoustic emission waves in carbon fiber reinforced polymer panels and directly obtained the amplitude attenuation formula by accounting for diffusion attenuation and absorption attenuation. Nevertheless, they lacked convincing theoretical derivation.

Overall, previous studies on the attenuation laws of acoustic emission waves did not consider the different forms of medium structures or failed to account for diffusion, scattering, and absorption attenuation. Moreover, most scholars tend to believe that amplitude attenuation presents an exponential function form. In particular, few have focused on the amplitude attenuation laws of acoustic emission waves in plate structures. In the present study, the traditional model of amplitude attenuation was improved, a power function model of amplitude attenuation in plate structures was established, and a pencil lead break (PLB) experiment was performed to validate the improved model. The results of this study will preliminarily reveal the laws governing the amplitude attenuation of acoustic emission waves in plate structures.

The remainder of this paper is organized as follows: In Section 3, the improvement of the traditional model of the amplitude attenuation of acoustic emission waves is discussed. This section also provides a discussion of the experimental verification of the improved model. The results of the multiple analyses of the improved mathematical model of amplitude attenuation through the curve fitting method are presented in Section 4. The summary and conclusions are provided in the final section.

3. METHODOLOGY

3.1. TRADITIONAL MODEL OF AMPLITUDE ATTENUATION AND ITS CORRECTION

Traditional studies on the amplitude attenuation of acoustic emission waves considered that acoustic emission waves are propagated in the form of plane waves. Plane waves do not experience diffusion attenuation, and their energy transfer loss is only caused by scattering attenuation and absorption attenuation.

The propagation of the acoustic emission of plane waves per unit area is shown in Fig. 1.

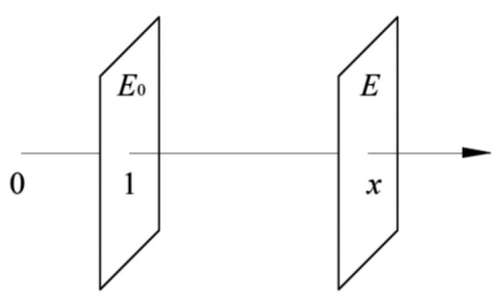

Fig. 1: Diagram of plane-wave acoustic emission

The energy loss per unit area caused by scattering attenuation and absorption attenuation is calculated as follows:

$$dE = -\alpha E dx \tag{1}$$

where α is the proportionality coefficient, and E is the energy of the acoustic emission of the wave at position x.

The following can be obtained by taking the integral of Eq. (1)

$$\int_{E_0}^{E} \frac{1}{E} dE = -\alpha \int_{1}^{x} dx \tag{2}$$

where E_0 is the unit energy of the acoustic emission source, namely, the wavefront energy per unit area at x=1.

Thus, the following equation can be obtained as follows:

$$E = E_0 e^{-\alpha} e^{-\alpha x} \tag{3}$$

The vibration energy of the particle m within this unit area is set as:

$$E = \frac{1}{2} m v^2 \tag{4}$$

where m is the mass of the particle per unit area, and v is the vibration amplitude of the particle per unit area.

By simultaneously solving Eqs. (3) and (4), the vibration amplitude of this particle is obtained as:

$$v = \sqrt{\frac{2E_0 e^{-\alpha}}{m}} e^{-\frac{\alpha}{2}x} = Ae^{-\beta x} \tag{5}$$

where A is the maximum amplitude, which is expressed as $A = \sqrt{\frac{2E_0 e^{-\alpha}}{m}}$, and β is the amplitude attenuation index, expressed as $\beta = \frac{\alpha}{2}$. As shown in Eq. (5), amplitude attenuation caused by scattering attenuation and absorption attenuation is traditionally modeled in the form of an exponential function.

In fact, the diffusion and propagation of acoustic emission waves around the plate structure will change energy density per unit area in the propagation direction. The signal amplitude caused by diffusion attenuation is assumed to be inversely proportional to the square root of the distance from the acoustic source. After the correction of the amplitude attenuation of Eq. (5), the corrected exponential functional amplitude attenuation model is obtained as follows:

$$v = \frac{B}{\sqrt{x}} e^{-\lambda x} \tag{6}$$

where the meanings of coefficients B and λ are similar to those of A and β in Eq. (5).

3.2. IMPROVED AMPLITUDE ATTENUATION MODEL

The model of the amplitude attenuation of acoustic emission waves in plate structures was improved to fully account for the effects of diffusion, scattering, and absorption on acoustic emission wave attenuation.

An isotropic plate with unit thickness was obtained, and the energy of acoustic emission waves was assumed to be uniformly propagated in the form of a cylindrical wavefront (Fig. 2).

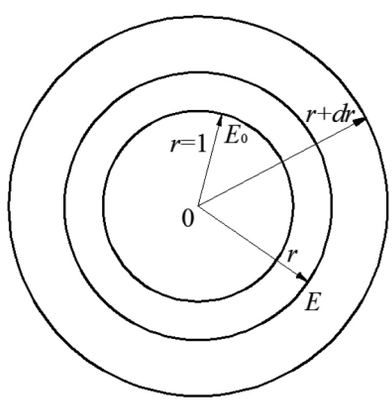

Fig. 2: Diagram of acoustic emission in the form of a cylindrical wavefront

The wavefront energy per unit area at position r is as follows:

$$e_x = \frac{kE}{r} \tag{7}$$

where k is the proportionality coefficient, r is the radius of the wavefront, and E is the unit wavefront energy at radius r.

The energy loss per unit area is assumed to be not only directly proportional to the propagation distance r of acoustic emission waves but also to the wavefront energy e_x per unit area at this position.

Then, the energy loss per unit area is as follows:

$$dE = -\frac{\alpha' kE}{r} dr \tag{8}$$

where a' is the proportionality coefficient related to medium grain size, anisotropy coefficient, and acoustic emission wave frequency.

The following formula is obtained by taking the integral of Eq. (8):

$$\int_{E_0}^{E} \frac{1}{E} dE = -\alpha' k \int_{1}^{x} \frac{1}{r} dr \tag{9}$$

where E_0 is the unit energy of the acoustic emission source and is defined as the energy of the unit wavefront at r=1.

The following is obtained:

$$E = E_0 x^{-\alpha' k} \tag{10}$$

The energy at any particle on the wavefront of r=x is as follows:

$$e = \frac{E_0}{2\pi x} x^{-\alpha' k} = \frac{E_0}{2\pi} x^{-(\alpha' k+1)} \tag{11}$$

The vibration amplitude at this particle is obtained in accordance with Eqs. (4) and (11):

$$v = \sqrt{\frac{E_0}{m\pi} x^{-(\alpha' k+1)}} = Dx^{-\gamma} \tag{12}$$

where D is the maximum amplitude and is expressed as $D=\sqrt{\frac{E_0}{m\pi}}$, and γ is the amplitude attenuation index and is expressed as $\gamma=\frac{\alpha' k+1}{2}$.

As shown in Eq. (12), the improved model of the amplitude attenuation of acoustic emission waves is in the form of a power function, and the values of coefficients D and γ are not constant. For example, if $\alpha'=0$, scattering attenuation and absorption attenuation are ignored, and only diffusion attenuation is considered. Then, γ is taken as 0.5, and Eq. (12) is simplified into:

$$v = Dx^{-0.5} \tag{13}$$

Eq. (13) indicates that the particle vibration amplitude caused by the diffusion attenuation of cylindrical waves is inversely proportional to the square root of the propagation distance. This conclusion is consistent with the hypothesis used to derive the corrected model in Section 3.1.

3.3. EXPERIMENTAL VERIFICATION

As revealed by the above theoretical study, the improved model of amplitude attenuation conforms to the attenuation laws of acoustic emission waves propagating in plate structures. The power function for the law of amplitude attenuation in plate structures was experimentally verified.

(1) Selection of the detection instrument

An experimental system for the attenuation of acoustic emission waves in an aluminum alloy plate was established (Fig. 3). The acoustic emission source was simulated through the PLB method, which provides the advantages of simplicity, economic efficiency, and favorable repetition.

Fig. 3: Experimental system for the attenuation of acoustic emission waves

A DS5 holographic acoustic emission signal analysis system from Beijing Softland Times Scientific & Technology Co., Ltd was used as the detecting instrument with the following concrete settings: channel threshold of 10 dB; preamplifier gain of 40 dB; peak definition time (PDT), hit definition time (HDT), and hit lockout time (HLT) of 1,000, 2,000, and 20,000 μm, respectively; and sampling frequency of 3 MHz.

(2) Setting of plate boundary conditions

The rectangular aluminum alloy plate was 2,455 mm in length, 1,220 mm in width, and 2 mm in thickness.

When both sides of the plate are air, the boundary conditions of the plate are considered to be a vacuum given the drastic differences between the acoustic impedances of aluminum alloy and air. Thus, the energy of acoustic emission waves would not be transferred beyond the plate structure.

When one or two sides of the plate are a solid medium, acoustic emission energy will be propagated to other solid media, further enlarging attenuation. Thus, setting the boundary conditions of the aluminum alloy plate during the experiment is necessary.

To ensure the normal propagation of acoustic emission waves in the aluminum alloy plate in the PLB experiment, the aluminum alloy plate was separated from the table with an underlayer of the minimum number of small foam boards.

(3) Selection and arrangement of sensors

The acoustic emission sensor was selected as R15α with the diameter of 19 mm, central frequency of 150 kHz, and frequency bandwidth of 50–400 kHz.

The sensors were arranged on the aluminum alloy plate in the order shown in Fig. 4 to measure the change trend of the amplitude attenuation of acoustic emission wave at different positions.

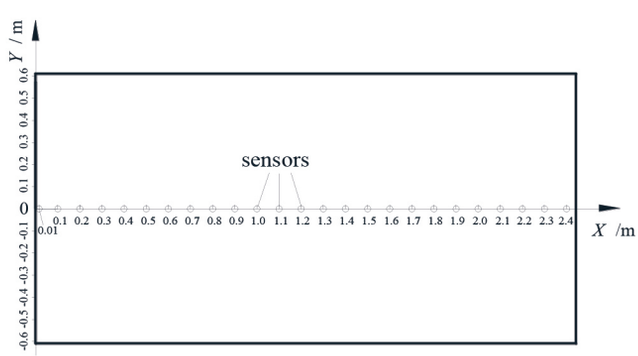

Fig. 4: Arrangement of experimental measuring points

A total of 25 measuring points were set in this experiment. The first measuring point was 0.01 m away from the original point, and the other 24 measuring points were equally spaced (0.1 m) from the original point. An appropriate amount of couplant was smeared between each sensor and aluminum alloy plate. Other clamping devices were not used.

(4) Selection of the PLB method

In accordance with the requirements of Hsu–Nielsen PLB method, the acoustic emission source was simulated through the breakage of a HB-type pencil core with a diameter of 0.5 mm. The length of broken core was 2.5 mm.

The lead-break position was selected at the left-end face of the aluminum alloy plate at the origin of coordinates. The direction of lead-break force was parallel to the upper surface of the plate, and the inclusion angle between the pencil lead and plate end face was 30°.

4. RESULT ANALYSIS AND DISCUSSION

4.1. EXPERIMENTAL SIGNAL PROCESSING

The acoustic emission waves underwent reflection, refraction, and pattern conversion as they propagated through the medium surface. As a result, complex signal data were acquired through the acoustic emission system. The waveform curve acquired by channel 8 of the acoustic emission system is shown as an example in Fig. 5 (a). Its spectrogram is shown in Fig. 5 (b).

As shown in Fig. 5 (a), the PLB signal waveform is a complicated waveform of multiple pulses or mutually superposed waveforms. It is formed through the separation of complicated sequences, such as longitudinal, transverse, surface or plate, and multiwave-path late waves. As shown in Fig. 5 (b), although the frequency range of the PLB signal is extensive, it mainly concentrates at approximately 150 kHz.

After the band-pass filtering of 100 to 200 kHz of the acoustic emission signals acquired at 25 measuring points, the first peak amplitudes (maximum value of the first amplitude peak) of the filtered signals were taken as attenuation measurement scales to verify the amplitude attenuation model of acoustic emission waves. This approach effectively avoided the disturbance caused by environmental noise to the first peak amplitudes of the measured signals and effectively reduced the effects of reflection and refraction of acoustic emission waves on the results of amplitude attenuation.

The original signals acquired by the first four channels of the acoustic emission system and first peak waveform curves after band-pass filtering are shown in Fig. 6 (a–d) (see section: supplementary material).

The data for the first peak amplitudes acquired at 25 measuring points of three PLB experiments were extracted and recorded in Table I (see section: supplementary material).

4.2. CURVE FITTING AND ANALYSIS OF FULL-FIELD ATTENUATION LAWS

To study the amplitude attenuation laws of the above PLB signal in the full field (from the acoustic source to the 24th measuring point), the improvement effect was verified through the curve fitting and analysis of the traditional exponential function, corrected exponential function, and improved power function models of amplitude attenuation.

The fitting diagrams for the first peak amplitude attenuation in the full field of the three PLB experiments, including the first peak amplitude ligature measured by the PLB experiment, fitted curve 1 of the traditional exponential function model, fitted curve 2 of the corrected exponential function model, and fitted curve 3 of the improved power function model, are shown in Fig. 7 (a–c) (see section: supplementary material).

As shown in Fig. 7 (a–c), the attenuation trends of the four curves are basically identical. The first peak amplitudes all gradually decrease with distance from the acoustic source. Moreover, attenuation rates decrease because high-frequency components attenuate faster than low-frequency components. Compared with fitted curve 1 of the traditional exponential function model, fitted curve 3 of the improved power function model and fitted curve 2 of the corrected exponential function model demonstrated favorable degrees of fitting with the data ligature measured through the PLB experiment. In particular, the fitting degree of fitted curve 3 is better than that of the other fitted curves.

Parameters, such as the sum of squared errors (SSE), root mean square error (RMSE), and R-square will be used to analyze experimental fitting conditions in detail. SSE is the square sum of errors between fitted data and original data of the measuring points, and RMSE is the square root of the mean of the square sum of errors between fitted data and original data of the measuring points. SSE and RMSE values close to 0 indicate good curve fitting effects and successful data prediction. R-square is the ratio of the quadratic sum of the difference between the mean values of predicted data and original data to the quadratic sum of the difference between original data and mean value. R-square values close to 1 indicate that the model fits the data well.

The fitting parameters of fitted curve 1 of the traditional model, fitted curve 2 of the corrected model, and fitted curve 3 of the improved model inferred from the data of three PLB experiments, as

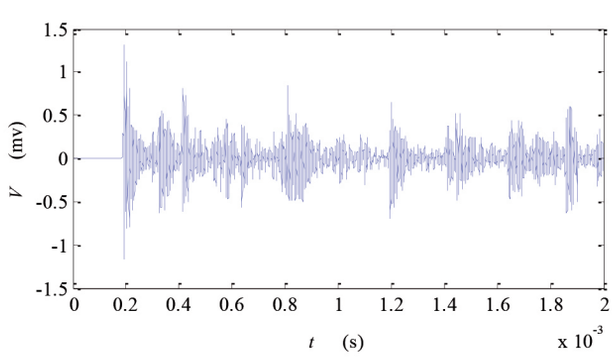

(a) The waveform curve

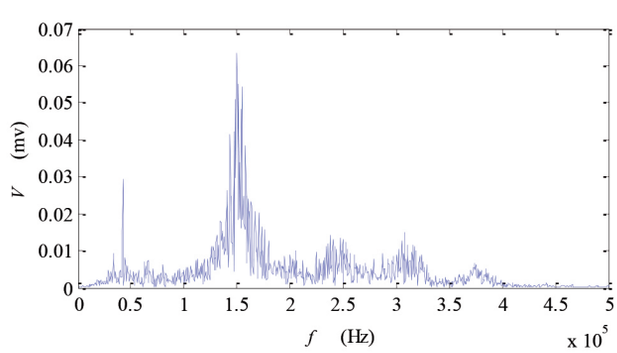

(b) The spectrogram

Fig. 5: Waveform curve of the eighth channel of the system

well as these mathematical models' coefficients, were calculated and are listed in Tables II to IV (see section: supplementary material).

The scale values of the fitting parameters of fitted curve 1 of the traditional model, fitted curve 2 of the corrected model, and fitted curve 3 of the improved model in the three PLB experiments are normalized to facilitate the discussion on the fitting conditions of the three models and are listed in Table V.

PLB Data	Proportions of Fitting Parameters of Curves 1, 2, and 3		
	SSE	RMSE	R-square
1	1:0.019:0.016	1:0.210:0.128	0.705:0.998:1
2	1:0.050:0.015	1:0.223:0.124	0.835:0.995:1
3	1:0.212:0.033	1:0.461:0.181	0.897:0.981:1
Mean	1:0.094:0.021	1:0.298:0.144	0.812:0.991:1

Table V Parameter proportions of the fitted curves of the three models

Table V clearly shows that the mean values of SSE and RMSE of the improved power function and the corrected exponential function models are 2.1% and 9.4% and 14.4% and 29.8%, respectively, of the traditional exponential function model. The two fitting parameters of the improved power function model and corrected exponential function model are significantly lower than those of the traditional exponential function model. This result indicates that the goodness of fit of the improved power function and the corrected exponential function models are better than that of the traditional exponential function model.

As shown in Table V, the mean SSE and RMSE values of the improved power function model are 22.3% and 48.3% of the corrected exponential function model, respectively indicating that the two parameters of the improved power function model are close to 0 and that the power function model better corresponds to the actual attenuation laws of acoustic emission waves in plate structures. This conclusion can also be obtained on the basis of the proportions of R-squares presented in Table V.

As shown in Table IV, the model coefficients D and γ that correspond to the three PLB data for the improved power function model of amplitude attenuation are considerably different. The drastic difference in values indicates that these coefficients are not constant and are dependent on propagation medium characteristics and wave source properties. These values can be obtained through the corresponding experimental analyses.

4.3. CURVE FITTING AND ANALYSIS OF NEAR- AND FAR-FIELD ATTENUATION LAWS

The acoustic emission field is divided into near field and far field in accordance with the distances of acoustic emission source and the sensor array. The amplitude attenuation laws of the propagation of the above PLB signals in the near-field and far-field will be studied.

(1) Division of near and far fields

The division of the near and far fields of acoustic emission waves lacks an absolute standard. When the distance from the acoustic source to central reference point of the sensor array is far greater than the acoustic wavelength, it is considered far field, otherwise, it is near field.

The empirical formula for the division of near and far fields is as follows [30]:

$$r = \frac{2d^2}{\lambda_{\min}} \tag{14}$$

where r is the distance from near-far-field boundary to the acoustic source; d is the distance between two neighboring sensors and is taken as 0.1 m; and λ_{min} is the minimum wavelength, which can be calculated on the basis of $\lambda_{\min} = \frac{C_L}{f_{\max}}$, where C_L is longitudinal wave velocity, f_{max} is the maximum frequency of acoustic emission waves, and the PLB signal frequency is taken as 333.3 kHz.

The theoretical velocity C_L of longitudinal waves of the aluminum alloy plate is as follows [31]:

$$C_L = \sqrt{\frac{E}{\rho}\frac{1-\nu}{(1+\nu)(1-2\nu)}} \tag{15}$$

where E is the elasticity modulus and is taken as 7.0×10^4 MPa; ν is Poisson's ratio and is taken as 0.3; and ρ is the density and is taken as 2.7×10^3 kg/m.

The empirical value for the division of the near and far fields in the PLB experiments was calculated to be r =1.1 m.

(2) Curve fitting and analysis of near field

The first peak amplitude data of the first 12 measuring points in the three PLB experiments are shown in Table I, and the near-

PLB Data	Function Type	SSE	RMSE	R-square
1	Traditional exponential function	1.019	0.319	0.794
	Corrected exponential function	0.035	0.059	0.993
	Improved power function	0.018	0.043	0.996
	Normalized proportion value	1:0.034:0.018	1:0.185:0.135	0.797:0.997:1
2	Traditional exponential function	3.170	0.563	0.874
	Corrected exponential function	0.150	0.123	0.994
	Improved power function	0.040	0.064	0.998
	Normalized proportion value	1:0.047:0.013	1:0.218:0.114	0.876:0.996:1
3	Traditional exponential function	4.048	0.636	0.920
	Corrected exponential function	0.772	0.278	0.985
	Improved power function	0.099	0.099	0.998
	Normalized proportion value	1:0.191:0.024	1:0.437:0.156	0.922:0.987:1
Mean normalized proportion value		1:0.091:0.018	1:0.280:0.135	0.865:0.993:1

Table VI Near-field fitting parameters of the three models

field data within $0 < r \leq 1.1$ m are taken as an example. The near-field amplitude attenuation fitting conditions of three PLB experiments are listed in Fig. 8 (a–c) (see section: supplementary material).

As shown in Fig. 8 (a–c), within the range of the near field, fitted curve 3 of the improved power function model exhibits the best degree of fitting with the data ligature measured through PLB experiments. The near-field fitting parameters of the three models are listed in Table VI.

As shown in Table VI, the SSE and RMSE mean values of the improved power function model are 19.8% and 48.2% of the corrected exponential function model, respectively. This result shows that the two fitting parameters of the improved power function model are significantly lower than those of the corrected exponential function model. Comparison with 22.3% and 48.3% of the corresponding data of the full field calculated indicates that the improved power function model is highly effective within the near field of acoustic emission waves in the plate structure.

(3) Curve fitting and analysis of far field

The first peak amplitude data of the last 13 measuring points in the three PLB experiments are shown in Table I. Far-field data within $1.1 < r \leq 2.4$ m are taken as an example. The far-field amplitude attenuation fitting conditions of three PLB experiments are provided in Fig. 9 (a–c) (see section: supplementary material).

As shown in Fig. 9 (a–c), within the far-field range, the differences among fitted curve 3 of the improved power function model, fitted curve 1 of the traditional exponential function model, and fitted curve 2 of the corrected exponential function model are negligible. The far-field fitting parameters of the three models are listed in Table VII.

As shown in Table VII, the differences among the SSE, RMSE, and R-square values of the three models are small and stable. This result indicates that all of the three models are effective models of acoustic emission waves in plate structures within the far-field range. Moreover, the normalized proportion data in Table VII show that compared with those of the other two models, the SSE and RMSE values of the traditional exponential function model are close to 0, and the R-square value is close to 1. This result indicates that the traditional exponential function model is more effective in describing the amplitude attenuation laws of acoustic emission waves within the far-field range.

The above experimental results show that the propagation of acoustic emission waves within the near and far fields of plate structures can be understood as follows: Within the near-field range, acoustic emission waves are considered cylindrical waves, and the gradual expansion of their wavefront gradually weakens energy and intensity. The analysis of their attenuation laws must consider the effect of diffusion attenuation in addition to scattering and absorption attenuation. Within the far-field range, acoustic emission waves can be regarded as plane waves, and the analysis of their attenuation laws must consider scattering and absorption attenuation and cannot ignore diffusion attenuation.

5. CONCLUSION

This study improved the traditional model of amplitude attenuation to reveal the laws governing the amplitude attenuation of acoustic emission waves in plate structures. It also identified the mathematical model applicable to the amplitude attenuation in plate structures. The amplitude attenuation model of acoustic emission waves in plate structures was theoretically investigated from the perspective of cylindrical waves. The suitability of the power function attenuation model was verified through the PLB experimental method with an aluminum alloy plate. Finally, the following conclusions were drawn:

(1) The amplitude and attenuation rate of acoustic emission waves in plate structures within full-field, near-field, and far-field ranges conforms to the power function model and gradually reduce as propagation distance increases.

(2) The corrected exponential function model provides a more reasonable description of amplitude attenuation laws within the full-field and near-field ranges than the traditional exponential function model. However, these models are less accurate than the power function model.

(3) The traditional exponential function model can appropriately describe the amplitude attenuation laws of acoustic emission waves only within the far-field range of acoustic emission waves in plate structures. Using this model to describe the amplitude attenuation laws of acoustic emission waves in the full-field and near-field ranges will result in drastic deviations.

The effects of diffusion, scattering, and absorption attenuation were considered in the analysis of the amplitude attenuation laws of acoustic emission waves within the full-field, near-field, and far-field ranges in plate structures. The results of this work provide theoretical guidance for development of the acoustic emission technology. However, the amplitude attenuation laws of acoustic emission waves are only applicable in isotropic plate structures, and its application in anisotropic plate structures remains limited.

This study shows that the mathematical model of the ampli-

PLB Data	Function Type	SSE	RMSE	R-square
1	Traditional exponential function	0.007	0.026	0.709
	Corrected exponential function	0.008	0.027	0.679
	Improved power function	0.008	0.028	0.667
	Normalized proportion value	0.875:1:1	0.963:0.964:1	1:0.958:0.941
2	Traditional exponential function	0.015	0.037	0.732
	Corrected exponential function	0.017	0.039	0.703
	Improved power function	0.017	0.040	0.690
	Normalized proportion value	0.882:1:1	0.949:1:1	1:0.960:0.943
3	Traditional exponential function	0.018	0.040	0.702
	Corrected exponential function	0.020	0.042	0.671
	Improved power function	0.020	0.043	0.660
	Normalized proportion value	0.9:1:1	0.952:0.977:1	1:0.956:0.940
Mean normalized proportion value		0.886:1:1	0.955:0.972:1	1:0.958:0.941

Table VII Far-field fitting parameters of the three models

tude attenuation of acoustic emission waves in plate structures can be used in the research of new methods for the acoustic source positioning of burst-type acoustic emission waves. Thus, this study may promote the development and application of acoustic emission technology.

REFERENCES

[1] Shen G T. "Acoustic emission technology and application". Beijing: Science Press. June 2015. p.1-20. ISBN: 978-7-030-44522-3

[2] Chou H Y, Mouritz A P, Bannister M K, et al. "Acoustic emission analysis of composite pressure vessels under constant and cyclic pressure". Composites Part A: Applied Science and Manufacturing. March 2015. Vol. 70. p. 111-120. DOI: http://dx.doi.org/10.1016/j.compositesa.2014.11.027

[3] Lee S B, Roh S M. "Developing an Early Leakage Detection System for Thermal Power Plant Boiler Tubes by Using Acoustic Emission Technology". Journal of the Korean Society for Nondestructive Testing. December 2016. Vol. 36-3. p. 181-187. DOI: http://dx.doi.org/10.7779/JKSNT.2016.36.3.181

[4] Liu M, Wang Q, Zhang Q, et al. "Characterizing hypervelocity (> 2.5 km/s)-impact-engendered damage in shielding structures using in-situ acoustic emission: Simulation and experiment". International Journal of Impact Engineering. April 2018. Vol. 111. p. 273-284. DOI: http://dx.doi.org/10.1016/j.ijimpeng.2017.10.004

[5] Holford K M, Eaton M J, Hensman J J, et al. "A new methodology for automating acoustic emission detection of metallic fatigue fractures in highly demanding aerospace environments: An overview". Progress in Aerospace Sciences. April 2017. Vol. 90. p. 1-11. DOI: http://dx.doi.org/10.1016/j.paerosci.2016.11.003

[6] C.U. Grosse, M. Ohtsu. "Acoustic emission testing-basics for research". Springer Verlag, Berlin & Heidelberg, Germany. January 2008. p. 3-10. DOI: https://doi.org/10.1007/978-3-540-69972-9

[7] Cheon D S, Jung Y B, Park E S, et al. "Evaluation of damage level for rock slopes using acoustic emission technique with waveguides". Engineering Geology. July 2011. Vol. 121-1-2. p. 75-88. DOI: http://dx.doi.org/10.1016/j.enggeo.2011.04.015

[8] Zelenyak AM, Hamstad MA, Sause MG. "Modeling of acoustic emission signal propagation in waveguides". Sensors (Basel, Switzerland). May 2015. Vol. 15-5. p. 11805-11822. DOI: http://dx.doi.org/10.3390/s150511805

[9] Li W, Kong Q, Ho S C M, et al. "Feasibility study of using smart aggregates as embedded acoustic emission sensors for health monitoring of concrete structures". Smart Materials and Structures. November 2016. Vol. 25-11. p. 115031. DOI: http://dx.doi.org/10.1088/0964-1726/25/11/115031

[10] Ni Q Q, Iwamoto M. "Wavelet transform of acoustic emission signals in failure of model composites". Engineering Fracture Mechanics. April 2002. Vol. 69-6. p. 717-728. DOI: https://doi.org/10.1016/S0013-7944(01)00105-9

[11] Morscher G N, Gyekenyesi A L. "The velocity and attenuation of acoustic emission waves in SiC /SiC composites loaded in tension". Composites science and technology. July 2002. Vol. 62.9. p. 1171-1180. DOI: http://dx.doi.org/10.1016/S0266-3538(02)00065-9

[12] Savoldi F, Tsoi J K H, Paganelli C, et al. "Evaluation of rapid maxillary expansion through acoustic emission technique and relative soft tissue attenuation". Journal of the Mechanical Behavior of Biomedical Materials. January 2017. Vol. 65. p. 513-521. DOI: https://doi.org/10.1016/j.jmbbm.2016.09.016

[13] Shehadeh M F, Abdou W, Steel J A, et al. "Aspects of acoustic emission attenuation in steel pipes subject to different internal and external environments". Proceedings of the Institution of Mechanical Engineers, Part E: Journal of Process Mechanical Engineering. February 2008. Vol. 222-1. p. 41-54. DOI: http://dx.doi.org/10.1243/09544089JPME143

[14] Zhao X M, Jiao L L, Zhao J, et al. "Acoustic emission attenuation and source location on the bending failure of the rectangular mortise-tenon joint for wood structures". Journal of Beijing Forestry University. January 2017. Vol. 39-1. p. 107-111. DOI: http://dx.doi.org/10.13332/j.1000-1522.20160150

[15] Wang X, Liang J, Qi K, et al. "Numerical simulation study on propagation law of acoustic emission signal of slewing ring". Advances in Acoustic Emission Technology. Springer, New York, NY. September 2015. p. 651-666. DOI: http://dx.doi.org/10.1007/978-1-4939-1239-1_60

[16] Hafizi Z M, Epaarachchi J, Lau K T. "An investigation of acoustic emission signal attenuation for progressive failure monitoring in fiberglass reinforced composite laminates". International Journal of Automotive and Mechanical Engineering. July-December 2013. Vol. 8-1. p. 1442-1456. DOI: http://dx.doi.org/10.15282/ijame.8.2013.31.0119

[17] Maillet E, Godin N, R'Mili M, et al. "Real-time evaluation of energy attenuation: A novel approach to acoustic emission analysis for damage monitoring of ceramic matrix composites". Journal of the European Ceramic Society. July 2014. Vol. 34-7. p. 1673-1679. DOI: http://dx.doi.org/10.1016/j.jeurceramsoc.2013.12.041

[18] Näsholm S P, Holm S. "Linking multiple relaxation, power-law attenuation, and fractional wave equations". Journal of the Acoustical Society of America. November 2011. Vol. 130-5. p. 3038-3045. DOI: https://doi.org/10.1121/1.3641457

[19] Capelli A, Kapil J C, Reiweger I, et al. "Speed and attenuation of acoustic waves in snow: Laboratory experiments and modeling with Biot's theory". Cold Regions Science and Technology. May 2016. Vol. 125. p. 1-11. DOI: http://dx.doi.org/10.1016/j.coldregions.2016.01.004

[20] Wang X H, Hu H W, Zhang Z Y. "Attenuation of acoustic emission signals in structural interfaces". Advanced Materials Research. Trans Tech Publications. September 2012. Vol. 569. p. 343-346. DOI: http://dx.doi.org/10.4028/www.scientific.net/AMR.569.343

[21] Zhang Y, Lu W X, Chu F L. "Faulted planet gear positioning based on attenuation characteristics of AE signals". Journal of Vibration and Shock. February 2017. Vol. 36-3. p. 14-19. DOI: http://dx.doi.org/10.13465/j.cnki.jvs.2017.03.003

[22] Manthei G, Eisenblatter J, Spies T. "Determination of wave attenuation in rock salt in the frequency range 1-100 kHz using located acoustic emission events". Progress in Acoustic Emission. 2006. Vol. 24. p. 179-186.

[23] Wang X, Liang J, Qi K, et al. "Numerical Simulation Study on Propagation Law of Acoustic Emission Signal of Slewing Ring. Advances in Acoustic Emission Technology". Springer New York, 2015. p. 651-666. DOI: http://dx.doi.org/10.1007/978-1-4939-1239-1_60

[24] Smith A, Dixon N, Fowmes G. "Monitoring buried pipe deformation using acoustic emission: quantification of attenuation". International Journal of Geotechnical Engineering. September 2017. Vol. 11-4. p. 418-430. DOI: http://dx.doi.org/10.1080/19386362.2016.1227581

[25] Li F, Huang L, Zhang H, et al. "Attenuation of acoustic emission propagation along a steel strand embedded in concrete". Ksce Journal of Civil Engineering. 2017. Vol. 5. p. 1-9. DOI: http://dx.doi.org/10.1007/s12205-017-0844-y

[26] Tang J, Lu W, Li Z, et al. "Attenuation characteristics of Lamb wave in carbon fiber reinforced composite laminated plate". Journal of Vibration and Shock. March 2016. Vol. 35-6. p. 75-79. DOI: http://dx.doi.org/10.13465/j.cnki.jvs.2016.06.013

[27] Sabzevari S A H, Moavenian M. "Sound localization in an anisotropic plate using electret microphones". Ultrasonics. January 2017. Vol. 73. p. 114-124. DOI: http://dx.doi.org/10.1016/j.ultras.2016.09.004

[28] Hafizi Z M, Epaarachchi J, Lau K T. "An investigation of acoustic emission signal attenuation for monitoring of progressive failure in fiberglass reinforced composite laminates". International Journal of Automotive and Mechanical Engineering. July-December 2013. Vol. 8. p. 1442. DOI: http://dx.doi.org/10.15282/ijame.8.2013.31.0119

[29] Asamene K, Hudson L, Sundaresan M. "Influence of attenuation on acoustic emission signals in carbon fiber reinforced polymer panels". Ultrasonics. May 2015. Vol. 59. p. 86-93. DOI: http://dx.doi.org/10.1016/j.ultras.2015.01.016

[30] Brandstein, Michael, Darren Ward. "Microphone arrays: signal processing techniques and applications". Springer, New York. 2001. DOI: http://dx.doi.org/10.1007/978-3-662-04619-7

[31] Malischewsky P G, Tuan T T. "A special relation between Young's modulus, Rayleigh-wave velocity, and Poisson's ratio". Journal of the Acoustical Society of America. December 2009. Vol. 126-6. p. 2851-3. DOI: http://dx.doi.org/10.1121/1.3243464

APPRECIATION

This research work was supported by the National Natural Science Foundation of China (No.U1534204, 11872256).

SUPPLEMENTARY MATERIAL

http://www.revistadyna.com/documentos/pdfs/_adic/8987-1.pdf